Caving 2026 – A van As, D Cumming-Potvin & J Wesseloo (eds)
© 2026 Australian Centre for Geomechanics, Perth, ISBN 978-1-7636842-3-2
doi:10.36487/ACG_repo/2645_95

# Numerical sensitivity models for Lift 2 design for Chuquicamata mine

**Catalina Álvarez [a,*], Alejandro Ramirez [a], Francisco Galvez [b]**

[a] *ITASCA, Chile*

[b] *Chuquicamata Division, Codelco, Chile*

## Abstract

*The Chuquicamata underground mine started production in May 2019 with the undercutting of the central macroblock (MB) of Lift 1, located approximately 200 m below the open pit bottom. At present, several macroblocks are in production and have experienced different operational challenges related to drift stability and cave stagnation. Orebody heterogeneity remains an ongoing challenge and is being addressed through continuous drilling and laboratory testing programs. Chuquicamata mine has been proactive in integrating field observations with three-dimensional (3D) numerical modelling to anticipate and manage geotechnical risks.*

*The numerical modelling framework for Lift 1 is based on a hybrid methodology combining FLAC3D and gravity flow, which has been calibrated against observed events and is actively used to assess the predictive performance of macroblocks within Lift 1. Early designs for Lift 2, located approximately 400 m below Lift 1, are currently being evaluated using limited field data, including uncertainties in stress conditions at depth. Anticipating cave performance and drift stability is a key first step in assessing the business case for alternative production level layouts.*

*This study describes the application of the hybrid modelling methodology to assess the expected performance of a single macroblock in Lift 2. Sensitivity analyses are carried out considering a plausible range of in situ stress conditions and rock mass strength variations. The results provide a practical tool for evaluating cave performance, anticipating geotechnical risks, and supporting the business case for Lift 2.*

**Keywords:** *block caving, Lift 2, Chuquicamata mine, gravity flow, FLAC3D*

## 1 Introduction

Chuquicamata underground mine began caving in May 2019, following the undercutting of the central macroblock of Lift 1, which is located approximately 200 m below the final open pit floor. Since startup, multiple macroblocks have entered production and have provided a growing empirical basis for evaluating cave propagation and drift stability. The Lift 2 (or Level 2) design is being evaluated approximately 400 m below Lift 1 (Figure 1) and therefore under a deeper, and potentially less favourable, stress environment. Production level layout, rock mass quality, structural control, and mining-induced stress redistribution must all be considered simultaneously for the business case for the next lift to be technically defensible.

The main engineering problem addressed in this study is selecting a production level footprint sufficiently robust to initiate and sustain cave propagation. The geotechnical data are limited for Level 2, resulting in significant uncertainty with respect to the ore column and in situ stress characterisations. Drift stability is not described in this paper.

[*] Corresponding author. Email address: catalina.alvarez@oneitasca.com

The Chuquicamata porphyry deposit is composed of three main units that are defined according to different degrees of alteration and mineralisation. The two most dominant rock units are PEK (potassic) and QIS (quartz sericitic), representing respectively the upper and lower bounds of rock mass strength expected in Level 2.

The orientation and magnitude of the principal stresses ($\sigma_1$) at Level 2 are still uncertain, although mine-scale calibration has narrowed the options to three stress scenarios.

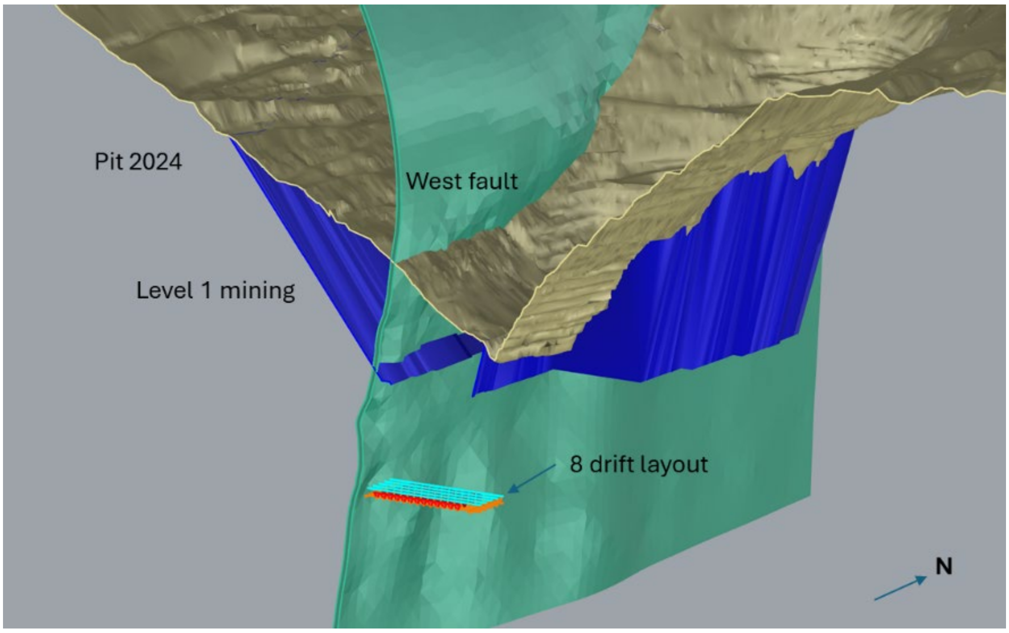


**Figure 1 Initial Level 2 geometry relative to Level 1 cave and the West Fault**

The paper builds on the coupled caveability methodology already used for the Lift 1 evaluations, in which FLAC3D (Itasca 2025a) is combined with MassFlow (Itasca 2025b) to resolve the mutual evolution of rock mass degradation, cavity growth, gravity flow and airgap generation.

Accordingly, the objective of the present work is to evaluate the expected performance of a representative Level 2 macroblock for three alternative production layouts containing 4, 6 and 8 drifts (Figure 2), under two alternative rock units (PEK or QIS). In turn, three different stress conditions are considered for each case (three layouts and two rock units).

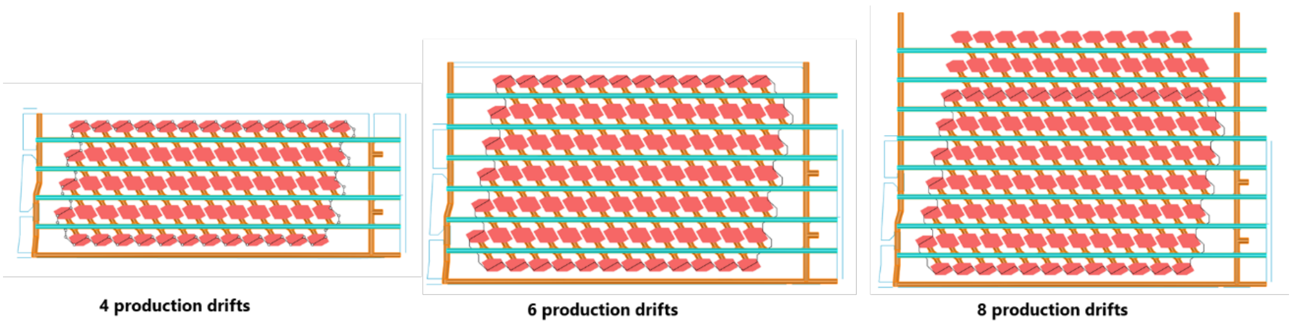


**Figure 2 Alternative footprint layouts (16 × 24 m pillar size)**

# 2 Methodology and numerical modelling

## 2.1 Production schedules and geotechnical characterisation

The production schedules for the three layouts use the same general development philosophy but different ramp-up durations and steady-state rates, as shown in Figure 3. Three footprint geometries were modelled under three different in situ stress states (Section 2.2), resulting in nine modelling cases in total. All cases use a 16.6 m undercut height. The mine plan therefore allows layout comparisons that separate geometric effects from production rate effects while still retaining a realistic ramp-up profile.

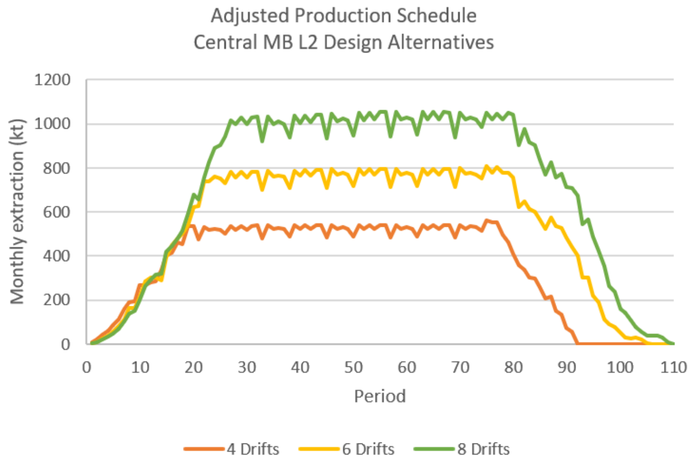


**Figure 3 Production schedule for the three alternative layouts**

To bound uncertainty in the Level 2 ore column, the analysis uses an auxiliary geotechnical unit with homogeneous intact rock properties representative of either QIS or PEK (Table 1). Geological strength index (GSI) is taken from the Level 2 block model in the auxiliary unit, whereas surrounding units retain mine-scale values from the current geotechnical model. When the auxiliary unit is treated as PEK, GSI increased by two points relative to the original block model, consistent with the current internal characterisation.

**Table 1 Intact rock properties for Level 2 analyses**

| Unit | Density (kg/m$^3$) | $E_i$ (GPa) | $\sigma_{ci}$ (MPa) | $m_i$ |
|---|---|---|---|---|
| QIS | 2,694 | 42 | 63 | 21 |
| PEK | 2,625 | 54 | 94 | 27 |

The structural model used in the mine-scale framework contains 149 faults, as shown in Figure 4. For the local macroblock model, 75 structures were retained explicitly as zone joints after trimming the model to cover the largest (8-drift) footprint. These structures were implemented explicitly in FLAC3D as zone joints. Fault strengths vary with friction between 25° and 30° and cohesion between 40 and 50 kPa, except for the regional structure known as the West Fault, which is characterised by 18° friction and 20 kPa cohesion.

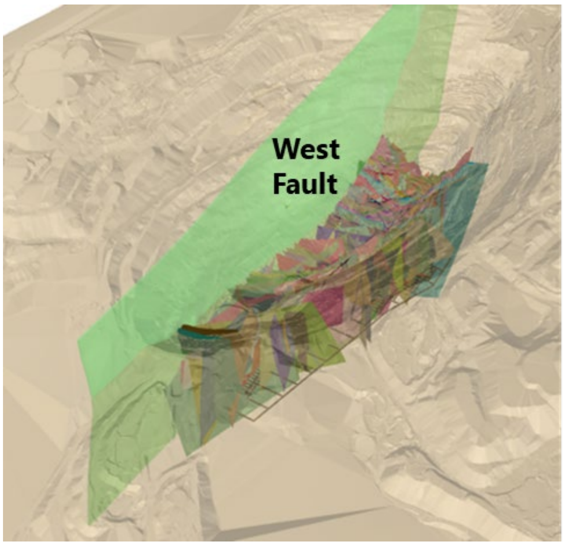


**Figure 4 Structural model for Chuquicamata underground mine**

## 2.2 In situ stress scenarios

Three pre-Level 2 mining stress conditions were considered for analysis. These scenarios, denoted 2023a, 2023b and 2021, differ in the orientation of $\sigma_1$ and in the magnitude of deviatoric stress at the planned production level. Figure 5 shows a stress profile for a point in the middle of Level 2 layout (production level elevation at 1,480 m or around 600 m below pit bottom). These stress conditions were obtained from mine-scale stress calibration analyses carried out over the last few years. As shown in Figure 5, the 2023a case is characterised approximately by $\sigma_1$ oriented north–south, the 2023b case is characterised by $\sigma_1$ oriented east–west, and the 2021 case by is characterised a sub-vertical $\sigma_1$. These fields were imported from the mine-scale model taking the 2024 open pit geometry and completed Level 1 mining into account. Note that the 2023b case carries the largest deviatoric stress ($\sigma_1$–$\sigma_3$) – nearly double that of the other two scenarios at Level 2 depth – which makes it the most favourable for yielding and cave initiation.

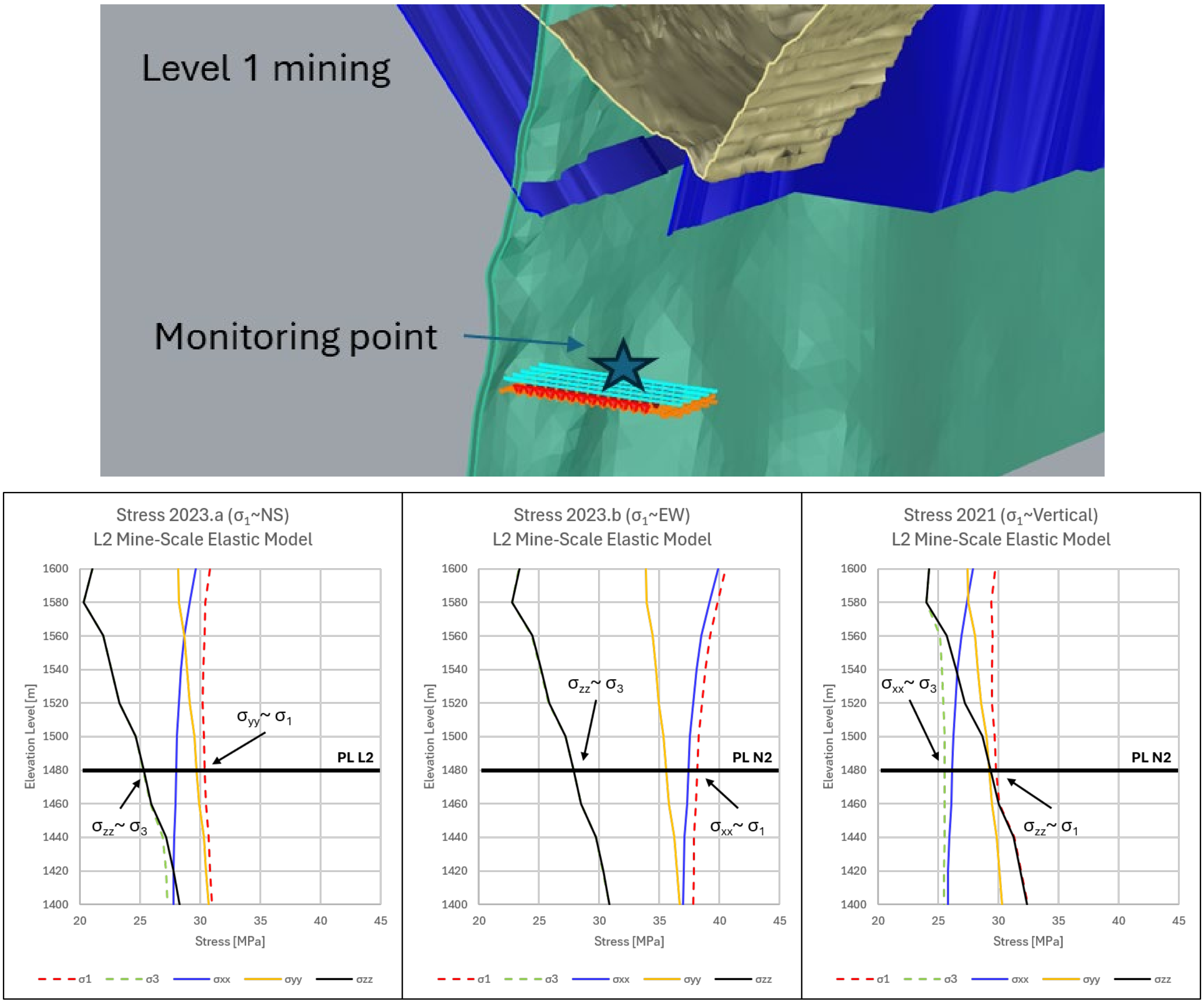


**Figure 5 Stress profile at monitoring point location (above) for the three stress scenarios considered prior to Level 2 mining**

## 2.3 Coupled MassFlow–FLAC3D framework

The study combines FLAC3D and MassFlow in a coupled workflow. FLAC3D resolves the evolving stress-deformation response and damage state of the rock mass, while MassFlow resolves the gravity flow, rilling, cavity geometry and airgap development associated with the draw. This coupling methodology is illustrated in Figure 6.

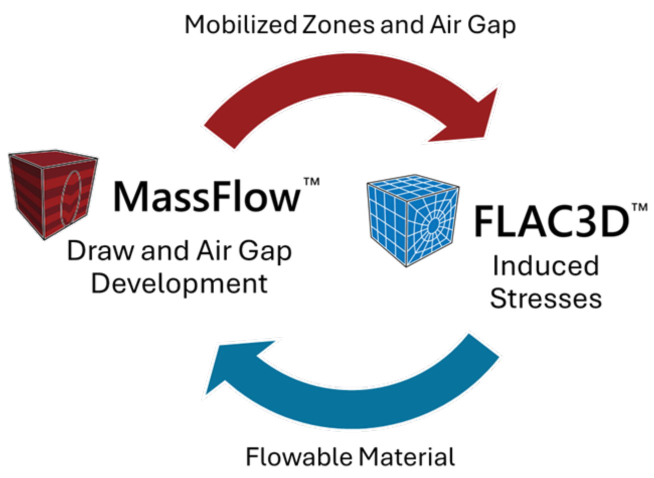


**Figure 6** **Schematic description of the numerical coupling**

The mechanical response was simulated in FLAC3D using IMASS (Itasca Model for Advanced Strain Softening), which reproduces cohesion weakening, tensile strength loss, frictional strengthening, modulus softening, density adjustment and bulking-related dilatancy. The Hoek–Brown failure surface was defined using the site-specific parameters $\sigma_{ci}$, $m_i$ and GSI, with disturbance factor D = 0 (Hoek et al. 2002). The rock mass stress-strain behaviour is illustrated in Figure 7, which shows the post-peak response, driven by the critical strain defined by Equation (1) (Lorig & Pierce 2000), where 'd' stands for model zone size and 'μ' is a calibration multiplier. For the caveability analyses, μ = 1.0 was retained from prior calibration against Lift 1 behaviour. The ultimate strength is driven by volumetric deformation (bulking).

$$\epsilon_{\text{crit}}^{p} = \left(\frac{12.5-0.125\times GSI}{100d}\right)\cdot \mu \tag{1}$$

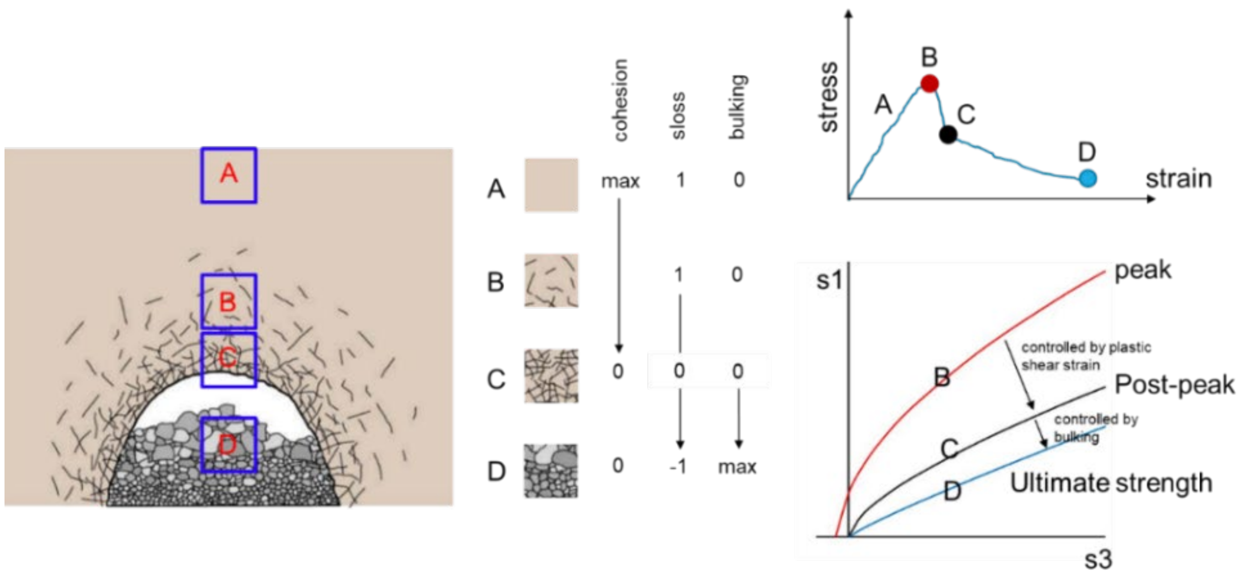


**Figure 7** **Schematic representation correlating various degrees of damage in a rock mass with the post-peak behaviour (points B, C and D) (Ghazvinian et al. 2020)**

The IMASS state variable sloss depicted in Figure 7 is an internal damage indicator representing the degree of rock mass softening/weakening within the IMASS constitutive model. It was used as a direct indicator of degradation, ranging conceptually from peak behaviour (approximately +1) through post-peak (approximately 0) towards residual strength (approximately −1). This variable is central to the coupled methodology because it links mechanical degradation in FLAC3D to material availability in MassFlow

(Figure 6). A zone was considered available to flow only when either one of two conditions was met: vertical settlement greater than 1 m or sloss < −0.01. The displacement threshold is consistent with comparable caving practice, whereas the sloss threshold is mine specific and was derived from previous calibration for Lift 1.

Two cave metrics were tracked through time, as defined in Figure 8. First, the cave back was defined directly from MassFlow markers representing air, bulked material and rilled material. Second, the fractured limit was defined by a total strain of approximately $5 \times 10^{-3}$, equivalent to an iso-surface of sloss near zero. The fractured limit advances ahead of the cave back, which makes it a useful indicator of impending connection and for estimating propagation rate before the cavity reaches the broken Level 1 material.

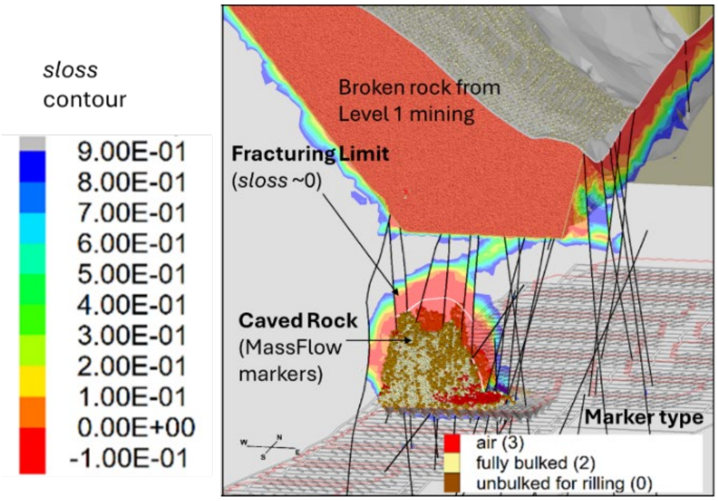


**Figure 8 Cave metrics as defined for the analyses**

The coupled analyses are developed within local model frameworks, considering stress initialisation states obtained from the open pit mine-scale stress model described previously, where three alternative stress conditions are considered. They represented the initial condition for the Level 2 underground analyses. The model is depicted in section views in Figure 9, indicating the location of the auxiliary unit representing the ore column material for Level 2. Figure 10 shows the GSI distribution for the sector, indicating values within 55–70 for the ore column.

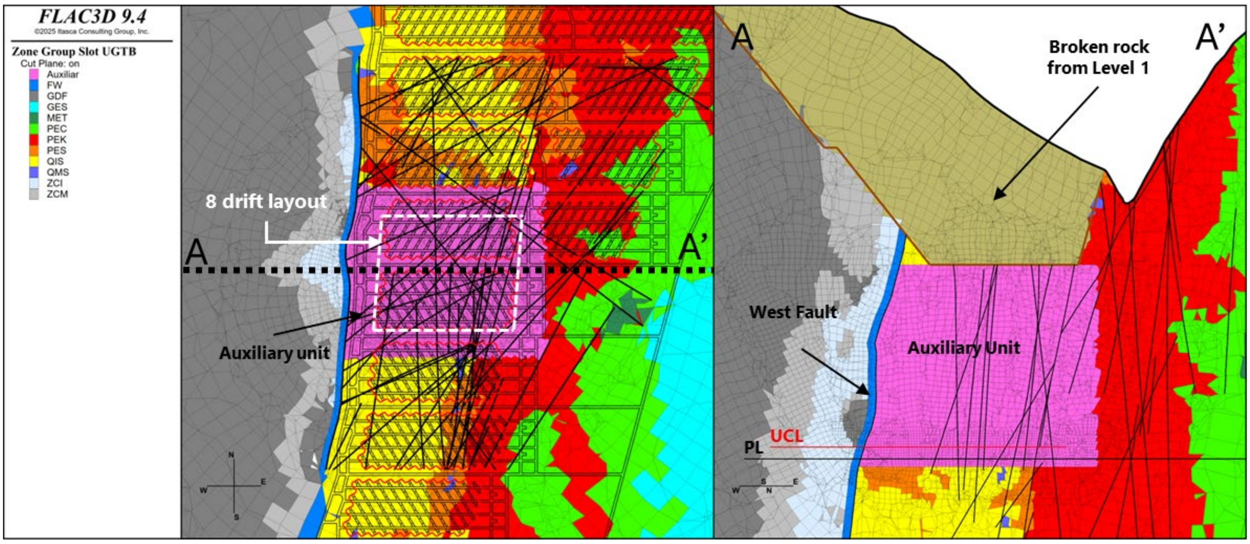


**Figure 9 Local FLAC3D model for coupled analyses**

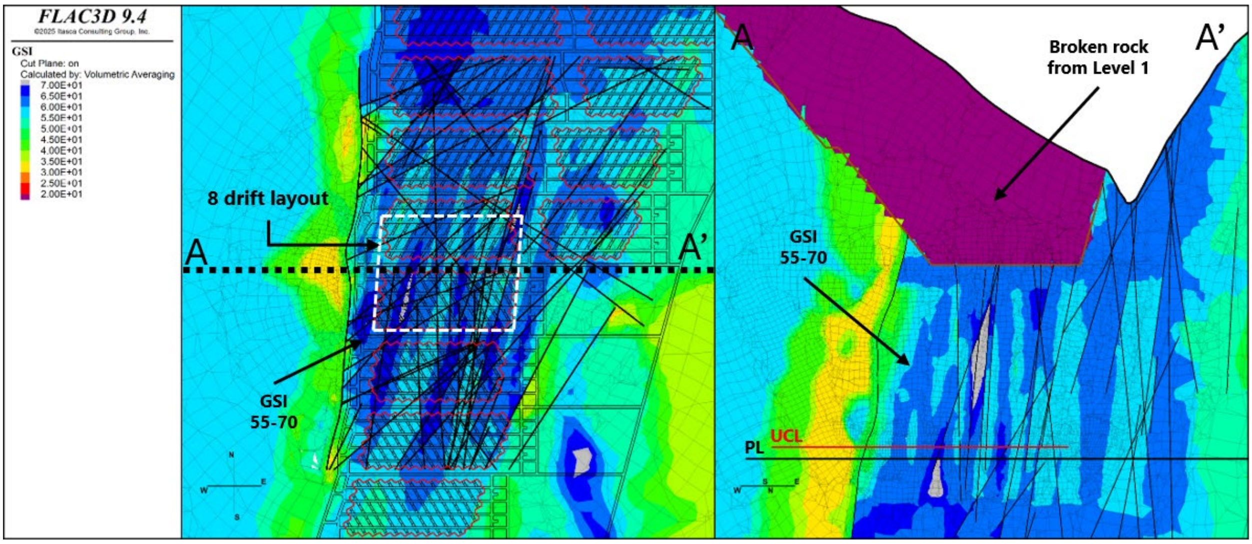


**Figure 10 GSI distribution obtained from block model**

# 3 Results and discussion

## 3.1 Cave propagation response in QIS

All nine QIS scenarios satisfied the practical criterion for cave propagation, defined here as the onset of sustained propagation before 100% of the drawbells are incorporated. Table 2 provides a summary of key outcomes for each case. Representative cave propagation results for the QIS stress scenarios, showing the influence of footprint size and stress orientation on cave geometry and timing, are given in Figures 11 and 12. As expected, the stress scenario with the largest deviatoric stress (2023b) provides the best response at the onset of caving propagation (smallest hydraulic radius, earliest propagation as measured by the percentage of footprint area). In other words, the east–west major principal stress promotes earlier yielding in the production column across all footprint sizes. As the footprint area increases, the absolute area required for initiation also increases, from 30,400 $m^2$ in the 4-drift layout to 36,000 $m^2$ in the 8-drift best case. This is equivalent to an increase in hydraulic radius, which shows that caving propagation requires a wider east–west coverage for the layouts with more drifts, requiring an open area that is closer in shape to a square than a rectangle. In terms of relative incorporated footprint area, the 8-drift layout under 2023b has the lowest percentage (47%) while the 4-drift layout has the highest percentage (77%).

In this study, each period represents one month of the production schedule. The propagation period is defined as the production period at which sustained upward growth of the caved zone is first observed, whereas the connection period corresponds to the onset of surface settlement greater than 1 m associated with cave breakthrough to surface. Propagation rates measured from the advance of the fractured limit range from about 5:1 to 7:1, indicating a progressive cave growth mechanism rather than a sudden collapse mechanism. Connection to Level 1 follows 5–9 propagation periods after initiation. Although 2023b is generally the most favourable stress case for initiation, the exact connection period remains strongly controlled by structure, which is why some 2023a and 2021 cases connect on comparable schedules after initiation has begun.

**Table 2 Summary of QIS caving response for the three layouts and three stress scenarios**

| Layout drift number | Stress scenario | Propagation period | Relative open area at cave propagation | Undercut area at cave propagation (m²) | Hydraulic radius (m) | Connection period |
|---|---|---|---|---|---|---|
| 4 | 2023a | 11 | 77% | 30,400 | 40 | 18 |
| | 2023b | 10 | 77% | 30,400 | 40 | 18 |
| | 2021 | 12 | 77% | 30,400 | 40 | 17 |
| 6 | 2023a | 13 | 62% | 36,500 | 44 | 18 |
| | 2023b | 11 | 57% | 33,400 | 42 | 20 |
| | 2021 | 13 | 62% | 36,500 | 44 | 19 |
| 8 | 2023a | 14 | 55% | 42,600 | 47 | 20 |
| | 2023b | 12 | 47% | 36,500 | 42 | 20 |
| | 2021 | 15 | 59% | 45,600 | 49 | 20 |

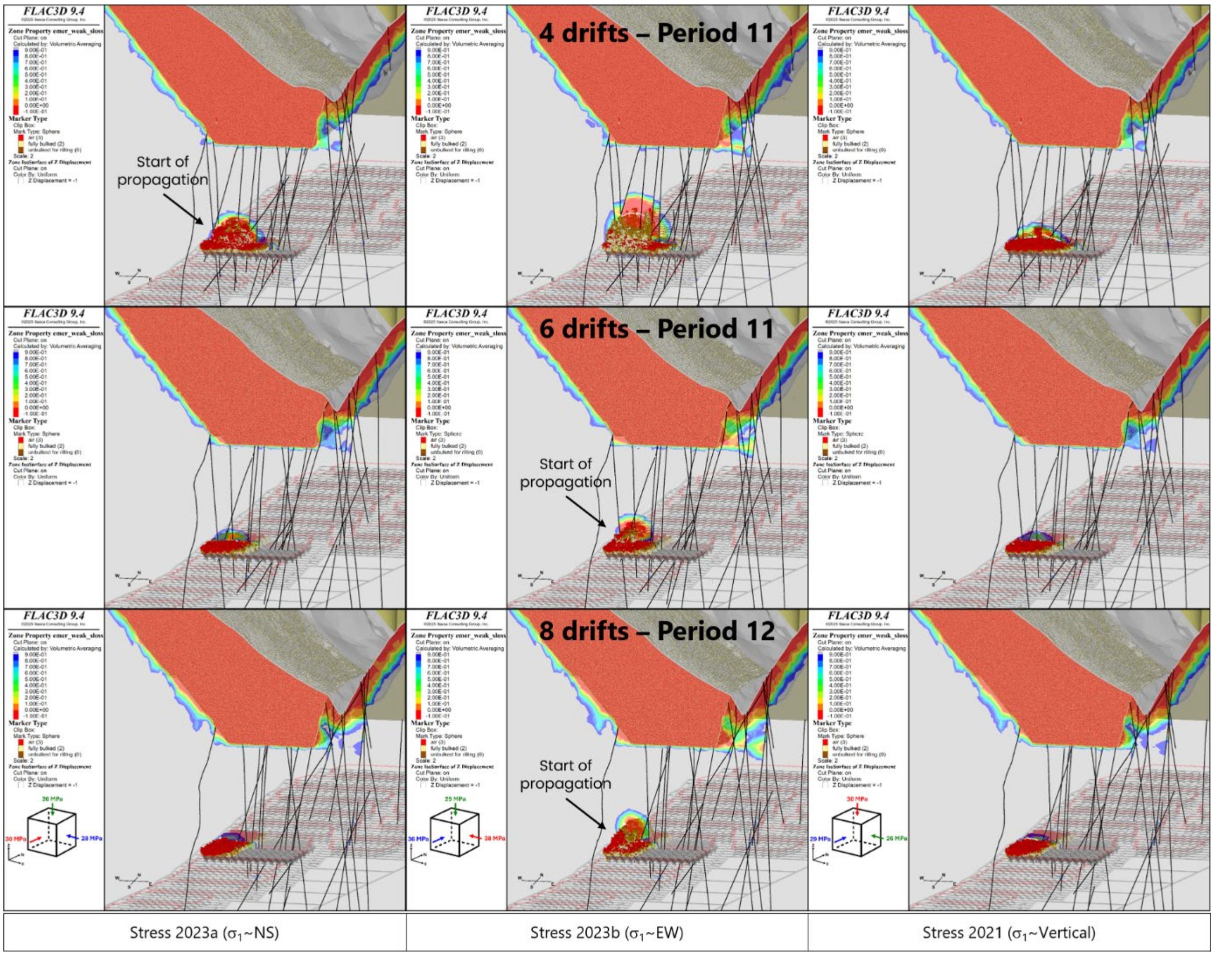


**Figure 11 Mining evolution at similar mining periods for all layouts (onset of propagation). Airgap shown in red markers and cross-section showing sloss contours (red colour representing weakened rock mass like broken rock) – QIS**

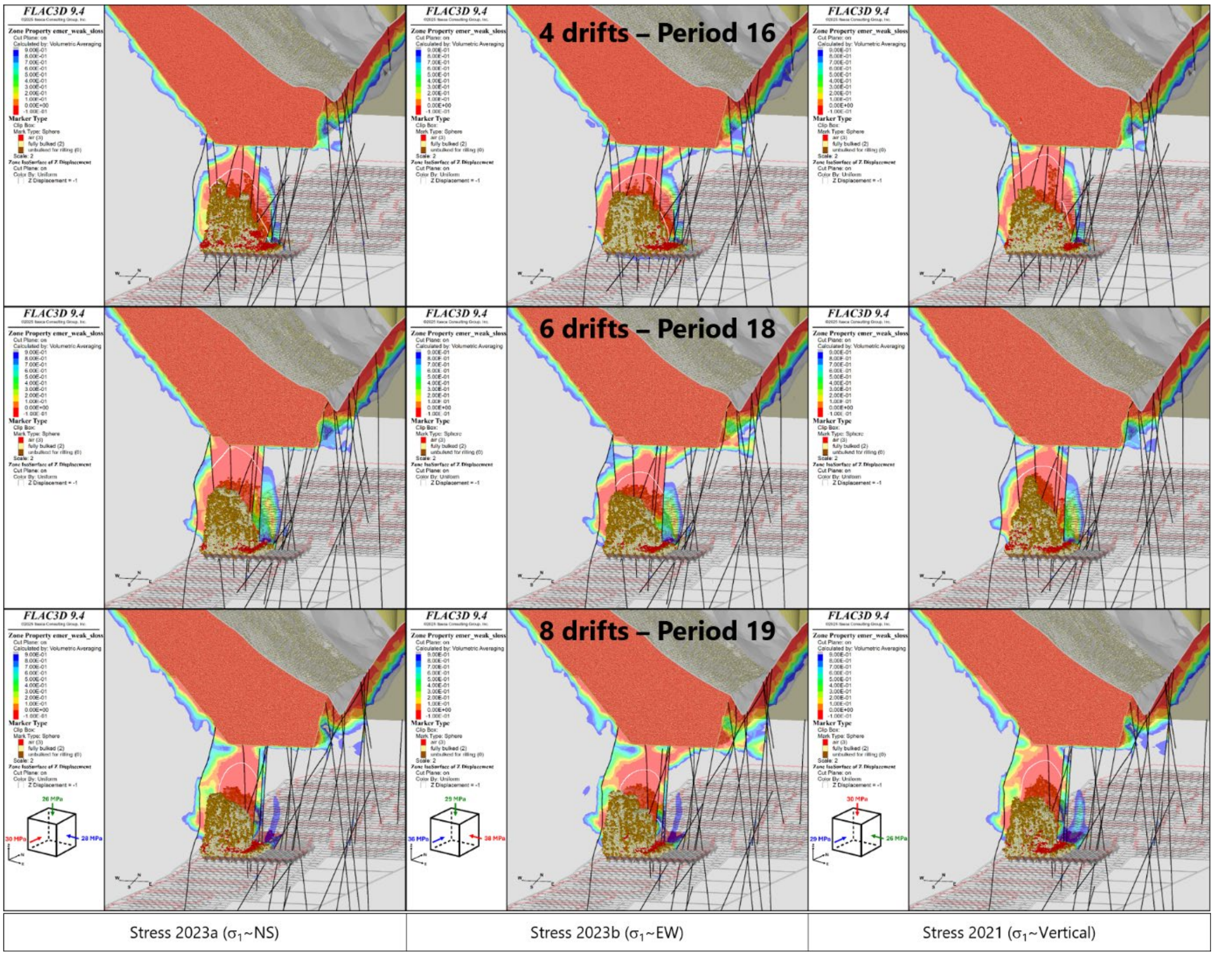


**Figure 12 Mining evolution at similar mining periods for all layouts (before reaching Level 1). Airgap shown in red markers and cross-section showing sloss contours (red colour representing weakened rock mass like broken rock) – QIS**

## 3.2 Cave propagation response in PEK

Only seven of the nine cases propagate, and the two non-propagating cases correspond to the 4-drift layout under the 2023a and 2021 stress fields. Table 3 provides a summary of the key outcomes related to each case. Representative cave propagation results for the PEK unit stress scenarios, showing the influence of footprint size and stress orientation on cave geometry and timing, are given in Figures 13 and 14. Even in the only successful 4-drift PEK unit case, propagation occurs when 100% of the footprint has been incorporated. The 6- and 8-drift PEK unit layouts do propagate under all three stress fields, but their response is delayed and mechanically more brittle than in the QIS unit. Initiation occurs in periods 19–27, at hydraulic radii of 49–61 m and incorporated areas of 45,600–66,880 m². The 2023b stress field again provides the most favourable conditions, with initiation at period 19 for both the 6- and 8-drift layouts and connection as early as period 21. By contrast, the 2021 case is the least favourable.

The most important distinction is not merely the delay in initiation, but the manner of propagation. PEK propagation rates in the period immediately preceding connection range only from 1:1 to 4:1. Combined with the lack of a stable, measurable intermediate propagation stage, these values indicate an abrupt transition from a relatively stagnant response to rapid upward breakthrough. That is a collapse-prone feature, and it implies that extraction rate planning and any future preconditioning strategy should be designed to avoid prolonged airgap growth followed by sudden cave back failure.

**Table 3 Summary of PEK caving response for the three layouts and three stress scenarios**

| Layout drift number | Stress scenario | Propagation period | Relative open area at cave propagation | Undercut area at cave propagation ($m^2$) | Hydraulic radius (m) | Connection period |
|---|---|---|---|---|---|---|
| 4 | 2023a | No propagation | – | – | – | – |
| | 2023b | 20 | 100% | 39,360 | 44 | 23 |
| | 2021 | No propagation | – | – | – | – |
| 6 | 2023a | 25 | 93% | 54,700 | 54 | 31 |
| | 2023b | 19 | 77% | 45,600 | 49 | 21 |
| | 2021 | 27 | 98% | 57,800 | 56 | 34 |
| 8 | 2023a | 23 | 78% | 60,800 | 58 | 27 |
| | 2023b | 19 | 67% | 51,700 | 53 | 21 |
| | 2021 | 26 | 86% | 66,900 | 61 | 30 |

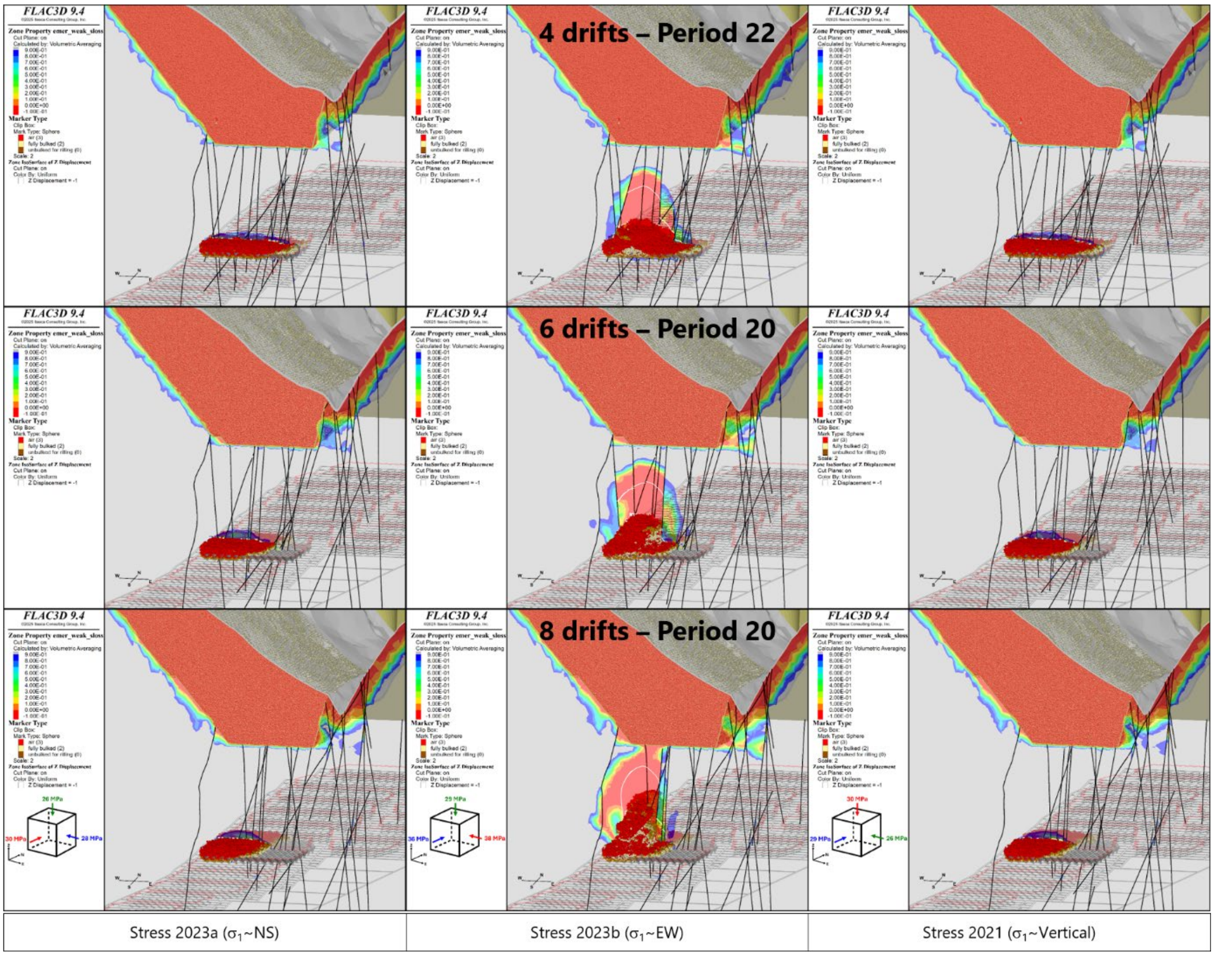


**Figure 13 Mining evolution at similar mining periods for all layouts (onset of propagation). Airgap shown in red markers and cross-section showing sloss contours (red colour representing weakened rock mass like broken rock) – PEK**

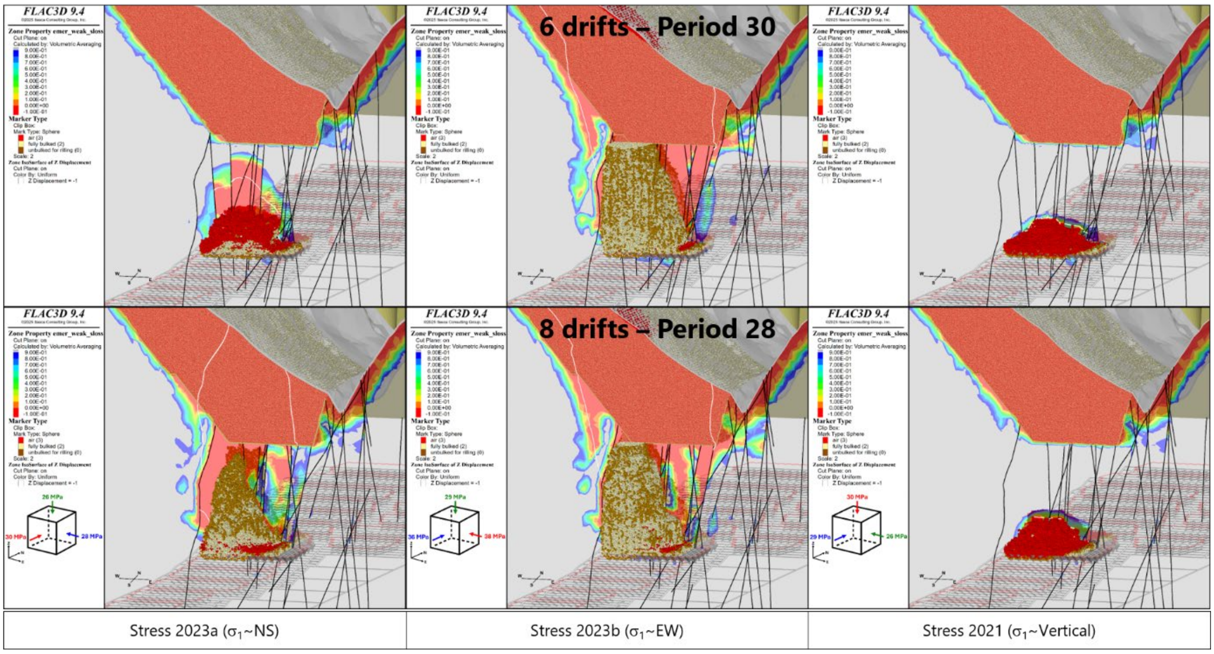


**Figure 14 Mining evolution at similar mining periods for 6 and 8 drift layouts (before reaching Level 1). Airgap shown in red markers and cross-section showing sloss contours (red colour representing weakened rock mass like broken rock) – PEK**

### 3.3 Structural control, propagation rate and cave management implications

A consistent finding across all layouts, material domains and stress scenarios is that cave geometry is structurally controlled. Sub-vertical faults confine the lateral extent of damage, while the West Fault acts as an effective western boundary to cave advance. As a result, the cave does not grow as an idealised axisymmetric column. Instead, it develops within a structurally filtered corridor where geometry changes with local stress and material properties. This observation matters operationally because it implies that simple footprint area metrics can be misleading if they are not interpreted in the context of structure-controlled cave shape.

Propagation rate provides an additional operational indicator than period to connection alone. In the QIS unit, the fractured limit advances with rates that remain in the same broad range at approximately half-height and immediately before breakthrough. That pattern is characteristic of progressive cave growth and is consistent with a manageable ramp-up environment. In the PEK unit, by contrast, intermediate rate measurement is generally not meaningful because the system tends to remain relatively stagnant before sudden acceleration. The modelled combination of low rates and abrupt breakthrough should therefore be treated as a precursor to potential roof collapse and potential airblast generation rather than as a benign delay.

By resolving both the broken rock cavity and the evolving air volume, the coupled workflow provides a basis to tie extraction rate during ramp-up to modelled propagation behaviour. For PEK-like responses, the results support conservative ramp-up and preconditioning alternatives that reduce the probability of prolonged stagnation followed by a potential abrupt collapse. For QIS-like responses, the same metric can be used to manage airgap development and to anticipate the timing of connection to the upper broken material.

## 4 Final remarks

The calibrated MassFlow–FLAC3D methodology provides a technically coherent way to evaluate the Lift 2 design at Chuquicamata because it resolves cave growth, broken rock mobilisation and airgap evolution within the same modelling framework.

In summary, if Level 2 conditions are closer to the QIS unit, caveability is robust across 4-, 6- and 8-drift footprints. If Level 2 conditions are closer to the PEK unit, the caveability becomes the limiting criterion, and the narrowest layout is not robust except under the most favourable stress condition. Under those conditions, either a wider footprint, preconditioning, or both, should be anticipated in the business case.

At an operational level, layout screening should remain conditional on updated stress measurements and improved geotechnical confidence at Level 2. PEK-like sectors should be evaluated together with preconditioning options and conservative ramp-up criteria.

Structural control is dominant in every scenario. Sub-vertical faults and especially the West Fault impose effective cave boundaries and therefore condition both the geometry and timing of propagation. Simple footprint metrics must therefore be interpreted alongside structural context.

## Acknowledgement

The authors thank Codelco for allowing publication of this paper.

## Use of artificial intelligence disclosure statement

In the preparation of this work, the authors used ChatGPT 5.4 for general assistance with writing and editing. The authors have reviewed the content, edited the text where required, and take full responsibility for said content.

## References

Ghazvinian, E, Garza-Cruz, T, Bouzeran, L, Fuenzalida, M, Cheng, Z, Cancino, C & Pierce, M 2020, 'Theory and Implementation of the Itasca Constitutive Model for Advanced Strain Softening (IMASS)', in R Castro, F Báez & K Suzuki (eds), *MassMin 2020: Proceedings of the Eight International Conference and Exhibition on Mass Mining*, University of Chile, Santiago, pp. 451–461.

Hoek, E, Carranza-Torres, C & Corkum, B 2002, 'Hoek-Brown failure criterion – 2002 edition', in R Hammah, W Bawden, J Curran & M Telesnicki (eds), *NARMS-TAC 2002: Mining and Tunnelling Innovation and Opportunity – Proceedings of the 5th North American Rock Mechanics Symposium and the 17th Tunnelling Association of Canada Conference*, vol. 1, University of Toronto Press, Toronto, pp. 267–273.

Itasca 2025a, *FLAC3D – Fast Lagrangian Analysis of Continua in Three-Dimensions*, version 9.4, computer software.

Itasca 2025b, *MASSFLOW – Analysis of Material Flow to Drawpoints*, version 9.4, computer software.

Lorig, L & Pierce, M 2000, *Methodology and Guidelines for Numerical Modelling of Undercut and Extraction Level Behaviour in Caving Mines*, report ICG00-099-6-15, report to the International Caving Study, October 2000, Itasca.